

PlanScope: Learning to Plan Within Decision Scope Does Matter

Ren Xin, Jie Cheng, Hongji Liu, and Jun Ma, *Senior Member, IEEE*

Abstract—In the context of autonomous driving, learning-based methods have been promising for the development of planning modules. During the training process of planning modules, directly minimizing the discrepancy between expert-driving logs and planning output is widely deployed. In general, driving logs consist of suddenly appearing obstacles or swiftly changing traffic signals, which typically necessitate swift and nuanced adjustments in driving maneuvers. Concurrently, future trajectories of the vehicles exhibit their long-term decisions, such as adhering to a reference lane or circumventing stationary obstacles. Due to the unpredictable influence of future events in driving logs, reasoning bias could be naturally introduced to learning based planning modules, which leads to a possible degradation of driving performance. To address this issue, we identify the decisions and their corresponding time horizons, and characterize a so-called decision scope by retaining decisions within derivable horizons only, to mitigate the effect of irrational behaviors caused by unpredictable events. Several viable implementations have been proposed, among which batch normalization along the temporal dimension is particularly effective and achieves superior performance. It consistently outperforms baseline methods in terms of driving scores, as demonstrated through closed-loop evaluations on the nuPlan dataset. Essentially, this approach accommodates an appealing plug-and-play feature to enhance the closed-loop performance of other learning-based planning models.

The source code and associated videos are available at <https://github.com/Rex-sys-hk/PlanScope>.

I. INTRODUCTION

Learning-based autonomous driving systems have been a promising approach for the popularity of unmanned vehicles. In particular, learning from driving logs of experts is broadly adopted to supervise neural networks for the planning task. During the training process, distance error is commonly employed, which is to measure the discrepancy between the planned state sequence and the expert demonstrations, thereby optimizing parameters of the neural network [1]. Yet, when training end-to-end autonomous driving systems, it is not entirely reasonable to set the logged expert states as target sequence, because future events are inherently uncertain, and potential disruptions such as unexpected obstacles or fluctuating traffic signals can significantly alter the trajectory planning. These unpredictable elements necessitate agile and nuanced adjustments to driving behavior. Some seemingly predictable decisions, such as behaviors in Game models with multiple Nash Equilibrium and switching traffic light, are difficult to accurately predict. Meanwhile, a short-sighted planner is also not desirable, as the planner also needs to keep its long-term decision in consideration when choosing

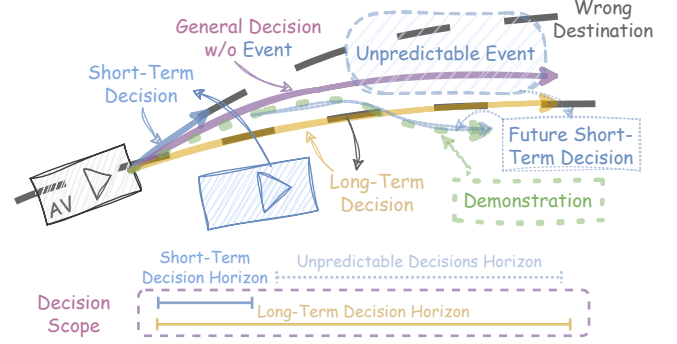


Fig. 1. In the scenario presented, the ego vehicle’s long-term decision-making is characterized by adherence to the reference line for driving. Conversely, short-term decision-making involves evading opposing vehicles through the application of lateral velocity. Long-term and short-term decisions integrate the general decision at the moment. However, the demonstrated trajectory, which anticipates future short-term decisions to avoid unpredictable events, may appear counterintuitive in the current context. The decision scope mechanism deliberately focuses on a limited horizon of short-term decisions while maintaining a broader horizon for long-term decisions, thereby mitigating the effect of unpredictable decisions in the demonstrated trajectory.

sudden maneuvers. Essentially, the state sequence of experts recorded in the log is a combination of short-term and long-term decisions under different scopes. A diagram of this concept is shown in Fig. 1. Due to the lack of observable information, long-term decisions are more susceptible to unpredictable events compared to short-term decisions. In learning targets like Average Distance Error (ADE), waypoints near the given current state only account for a small proportion of error compared to remote ones. This will result in a situation where unpredictable events occurring at the distant future affect current short-term decisions unexpectedly. This issue is evident during the training phase of the planning model, where it can lead to uneven convergence priorities or errant convergence over time. Therefore, considering the decision scope (DS) in the model training phase is crucial for making more intelligent planning decisions.

Addressing the decoupling issue of information from various decision scopes within the learning-from-demonstration framework presents significant challenges. Traditional planning methods divide the problem into distinct layers: path planning, behavior planning, and motion planning. Each of these layers is handled by specialized modules. In contrast, learning-from-demonstration approaches often focus on learning future trajectories of a fixed length. This focus arises because nuanced adjustment components and long-term decision components are difficult to separate from log replay. One potential solution is to employ manual annotation for driving behavior reasoning. This method can help analyze

Ren Xin, Jie Cheng, Hongji Liu, and Jun Ma are with The Hong Kong University of Science and Technology, Hong Kong SAR, China. (email: rxin@connect.ust.hk; jchengai@connect.ust.hk; hliucq@connect.ust.hk; jun.ma@ust.hk)

both long-term and short-term decisions, allowing for the identification of behavior duration and starting times. However, this approach entails a substantial workload and poses scalability challenges. Consequently, finding a cost-effective way to decouple decision scopes in the age of learning-based planning remains a complex issue that requires further exploration.

Three viable strategies are investigated in this work: 1) Assigning weight to the time dimension of loss; 2) Monitoring tracks through decisions of varying scales; and 3) Enabling the model to refine trajectories from coarse to fine. In our examination of time-dependent weighting methods, three approaches are proposed: time truncation, uncertainty-dependent weighting, and time-dependent normalization. These weights are incorporated into the computation of planning regression loss. For monitoring decision scales, we suggest that the model can learn to make decisions across different scopes by employing downsampling and truncation. Alternatively, the model can extract components of varying frequencies from expert trajectories using wavelet decomposition and adjust them according to planning requirements. Regarding the model structure for generating decisions at different scopes, both one-time and iterative generation methods are explored, which enable the model to refine trajectories from coarse to fine. To ensure a comprehensive and effective exploration, experimental validations of these strategies are conducted. Through our experiments, the most effective method is identified for enhancing model performance in closed-loop evaluations.

In summary, our contributions are threefold:

- We introduce PlanScope, a framework for formulating problems on training the sequential decision-making model, and demonstrate its impact by closed-loop evaluations.
- We explore a variety of methods under PlanScope framework in the aspects of learning weight calculation, trajectory decomposition, and the modeling structure of detail generation. Through comparative experiments, the most effective strategies are identified for enhancing trajectory execution performance.
- We extensively evaluate our method on the nuPlan [2] dataset, and the results demonstrate that it achieves superior driving scores compared to baseline methods in closed-loop none-reactive simulations (CLS-NR).

II. RELATED WORKS

A. Horizon Related Planner Design

Sequential decision-making can be encapsulated with the framework of Partially Observable Markov Decision Processes (POMDPs) [3]. For tasks with fixed decision horizons, this framework requires exponentially increasing search volume to find a feasible solution. However, in autonomous driving scenarios, in-time reaction and predictive decision are both required, making it challenging to determine the optimal policy sequence in real-time [4]. Hence, under traditional planning frameworks, hierarchical structure is typically employed to

streamline computations [5], [6]. In the hierarchical structure, the planning problem is decomposed across various frequency bands, each with distinct hierarchical tendencies. For large-scale exploration, one might opt for a lower resolution and focus on non-real-time targets. Conversely, within the smaller scale areas identified by the large-scale search, the planner can leverage higher resolution and account for dynamic objects that are impractical to predict accurately. In [7], the authors adapt this concept to the prediction phase, and segments the forecast for the subsequent four seconds into two stages. Initially, it meticulously predicts the agent's reachable area at 0.1-second intervals for the first 0.5 seconds. Subsequently, for the remaining 3.5 seconds, it utilizes an adaptive filter to depict potential vehicle positions. This approach allows the agent to maintain safety at a fine scale while preserving adaptability at a broader scale. In terms of learning-based planning, analogous strategies can be harnessed to simplify calculations and enhance performance. For instance, the Negative Log Likelihood (NLL) Loss, which is frequently utilized in predictive tasks [8], assigns greater uncertainty to long-term trajectory points, such that the scarcity of future information can be reflected. This phenomenon of probabilistic regression result helps to posit that historical trajectories provide limited insight, sufficient only for fine-tuned operations in the short term and for general directional guidance in the long term. However, NLL loss or probabilistic predictions are incompatible with the planning module, which necessitates deterministic outputs for trajectory followers. It leaves an open and interesting problem to develop an approach to address this challenge in trajectory planning. Essentially, there is a critical need for a method that accurately reflects the significance of decision components in trajectories or can extract them effectively.

B. Applications of Wavelet Transformation

Wavelet transformation is a potent tool in signal processing [9], [10]. This approach has been extensively applied in medical imaging and image recognition, which demonstrates superior performance comparing to convolutional neural networks (CNNs), particularly with fewer samples [11]. Its utility can be further extended to the domain of autonomous driving, where it has been effectively harnessed. For instance, in [12], wavelet transformation is employed to distill large-scale car-following behaviors. It preprocesses the signal approximations derived by wavelet transformation, calculates affinities using Summed Square Error (SSE), and identifies three predominant behavioral patterns through hierarchical clustering. In [13], vehicle state records are analyzed by wavelet transformation to identify drivers. Wavelet coefficients, energy, and statistical quantities are concatenated to the feature vector and recognized by classifiers like XGBoost, achieving around 100% accuracy when identifying 80% drivers. In [14], rasterized high-resolution maps are decomposed into multi-resolution geometry graphs by wavelet based cell decomposition. The graph is utilized by both path and motion planning modules to improve computing efficiency. Motivated by these precedents, we advocate the application of wavelet transformation to glean

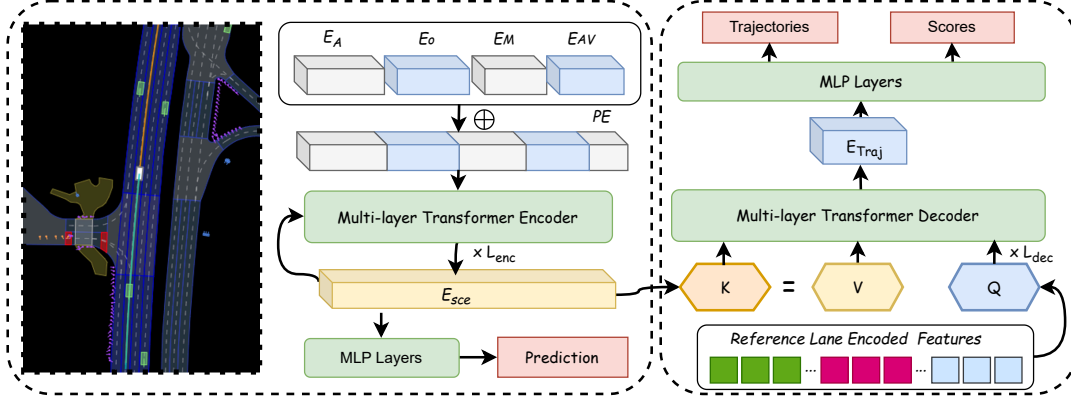


Fig. 2. The overall model framework initiates with the individual embedding of driving context elements, including the Ego Vehicle, Dynamic Agents, Static Objects, High-Definition Map, Traffic Signs, and Signals, followed by their concatenation with positional embedding (PE) [15]. This concatenated context is subsequently processed through a Multi-layer Transformer encoder, iterated L_{enc} times. The scenario embedding is then decoded to formulate agent predictions, which serve to comprehensively supervise the model's understanding of the driving context. The reference lane embedding and anchor-free variables are combined to form a query for the scenario embedding.

valuable information from expert trajectories.

III. METHODOLOGY

A. Problem Formulation & System Overview

Our research concentrates on addressing the problem of urban autonomous driving. At each time step, the autonomous vehicle is tasked with planning a future trajectory \mathcal{T} under various traffic-related contexts C_t . Each trajectory point has six channels: $[p_x, p_y, \cos \theta, \sin \theta, v_x, v_y]$. Driving contexts encompass dynamic agents (A), static objects (O), and Vectorized High-Definition Map (M) information. Generated outputs at time step t , denoted as G_t , include motion predictions \mathcal{P} of other agents, a multimodal trajectory score \mathcal{S} , and detailed trajectory information \mathcal{D} at different levels of detail. A basic mathematical formulation of this framework can be represented as follows:

$$C_t = \{A_t, A_t - 1, \dots, O_t, M_t, AV_t\}, G_t = \{\mathcal{T}, \mathcal{P}, \mathcal{S}, \mathcal{D}\},$$

$$G_t = f(C_t | \theta), \text{ w.r.t. } \theta = \arg \min_{\theta} \mathcal{L}(G_t, \hat{G}_t),$$

where f denotes the Neural Network (NN) model, θ is the model parameter, \mathcal{L} is the loss function, and \hat{G}_t is the ground truth of G_t from logged context.

Driving contexts are encoded as E_A, E_o, E_M, E_{AV} by Feature Pyramid Network (FPN) [16], Multi Layer Perceptron (MLP), PointNet [17] based vector encoder and attention based State Dropout Encoder (SDE) [18] respectively. As depicted in Fig. 2, the encoder section of our framework is conventional and similar to that of the baseline prediction and planning model described in [19]. The decoder section has been meticulously designed by us. It generates trajectories that are subsequently employed as references by a Linear Quadratic Regulator (LQR). To minimize the influence of human-defined rules, we have eliminated the rule-model hybrid post-processing module in our experiments. During the training phase, various commonly utilized auxiliary losses are integrated to supervise the trajectory generation. The training losses include prediction loss \mathcal{L}_{pre} , and collision loss \mathcal{L}_{col} ,

which can be expressed by

$$\mathcal{L}_{pre} = \text{L1}_{smooth}(\mathcal{P}, \hat{\mathcal{P}}),$$

$$\mathcal{L}_{col} = \frac{1}{T_f} \sum_{t=1}^{T_f} \sum_{i=1}^{N_c} \max(0, R_c + \epsilon - d_i^t),$$

where \mathcal{L}_{pre} calculates the future trajectory discrepancy between generated and that from dataset, \mathcal{L}_{col} computes the invasion distance using N_c circle represented vehicle outline in future T_f steps as described in [19], R_c is the summed radius of ego and agents outline circle, ϵ is the tolerance, and d_i^t represents the center distance between outline circles at time step t . Drawing inspiration from [20]–[22], the decoder's query is formulated as a concatenation of the reference lane encoding and anchor-free variables. The reference lane encoded features are concatenated with anchor-free learnable queries and serve as the initial query Q_0 to the scenario encoding within multi-layer transformer decoding operations, facilitating the generation of residual quantities of Q for subsequent layers. In training process, the final query Q_N is then forwarded to the trajectory MLP decoder and scoring MLP decoder, yielding the multi-modal trajectory and the score by

$$\mathcal{T} = \text{MLP}(Q_N), \pi = \text{MLP}(Q_N),$$

$$\mathcal{L}_{cls} = \text{CrossEntropy}(\pi, \hat{\pi}),$$

where $\hat{\pi}$ is a one hot vector indicating the trajectory closest to logged trajectory. Finally, the overall training loss is designed as

$$\mathcal{L} = \mathcal{L}_{reg} + \mathcal{L}_{cls} + \mathcal{L}_{pre} + \mathcal{L}_{col} + \mathcal{L}_{ds},$$

where \mathcal{L}_{reg} is the weighted regression loss and \mathcal{L}_{ds} is the loss to supervise learning within decision scope. More details on weights design, acquisition of supervision signals and the decoding of detailed information are elaborated in Section III-B, Section III-C and Section III-D.2, respectively.

B. Weighted Supervision

Using time-dependent weight along decision sequence is a promising way to express the importance of waypoint accuracy

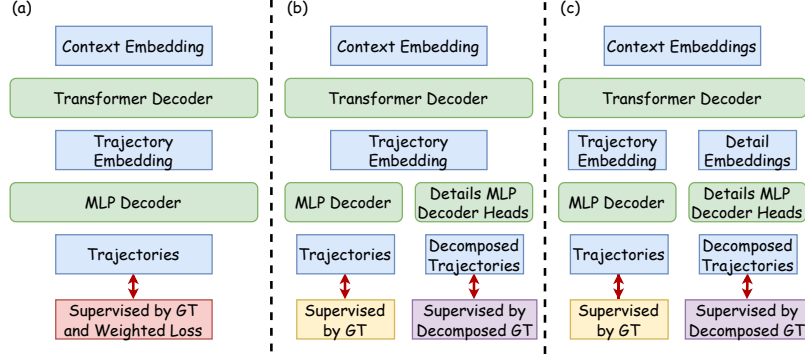


Fig. 3. Frameworks for achieving multi-scope trajectory supervision are illustrated in (a), (b), and (c). In (a), the trajectory is generated using the baseline framework but is supervised by a loss function with time-dependent weights. In (b), the last trajectory embedding is used not only to generate the full trajectory but also to map to the decomposed trajectory. In (c), multi-scope detail embeddings are iteratively generated during the decoding process of the Transformer Decoder.

in the learning process as shown in Fig. 3 (a). The weighted regression loss can be calculated by

$$\mathcal{L}_{\text{reg}t} = \text{L1}_{\text{smooth}}(\mathcal{T}_t, \hat{\mathcal{T}}_t),$$

$$\mathcal{L}_{\text{reg}} = \frac{1}{T} \sum_{t=0}^T \mathcal{L}_{\text{reg}t} \times w_t,$$

where w_t can be designated by the following methods:

1) *Time Truncation*: Only consider regression loss of first T time steps. In implementation, we also shorten the executed trajectory to eliminate the effect of uncontrolled waypoints. Mathematically,

$$w_t = \begin{cases} 1, & t < T, \\ 0, & t \geq T. \end{cases}$$

2) *Decreasing Certainty*: Those unpredictable disturbances might affect convergence capability on more important features and information for immediate decision. To describe this problem, we assume the sequential decision process conforms to the Gaussian Process (GP). GP is a non-parametric Bayesian method used to model functions. It assumes that any finite collection of function values follows a joint Gaussian distribution. For trajectory planning of an autonomous vehicle, the trajectory points $\mathbf{y}(t)$ can be modeled as outputs of a GP, with the mean and covariance determined by a kernel function $k(t_i, t_j)$, which can be a Radial Basis Function (RBF). Assuming the current state is an observable point, the variance of the predicted point at t can be easily derived by

$$\sigma_t^2 = \sigma_f^2 \left[1 - \exp\left(-\frac{(t - t_0)^2}{l^2}\right) \right],$$

where σ_f^2 is the function uncertainty, which can also be considered as the maximum uncertainty, l is the time length scaler, t_0 is the observable current time, which is set to 0 in the calculation. We define the uncertainty compensation as the deviation of maximum uncertainty. Mathematically,

$$\text{Compensation}(t) = \sigma_f^2 - \sigma_t^2.$$

Then, the calculation of weights to regularize uncertainty at each time point and can be simplified as

$$w_t = \frac{1}{Z} \exp\left(-\left(\frac{t - t_0}{l}\right)^p\right),$$

where Z is the average weight. p is the order of the time difference measurement, which is 2 for RBF.

3) *Time Dependent Normalization*: Normalization is a straight forward method to convert value of data to the same order of magnitude or limits it to a certain range. Borrowing the idea of Batch Normalization (BN), the average error e_t of each time step across the mini-batch can be dynamically calculated by

$$\text{BN}(e_t) = \frac{e_t - \mu_{B;t}^{e_t}}{\sigma_{B;t}} = \frac{e_t}{\mu_{B;t}^{|e_t|}}, \text{ when } \mu_{B;t}^{e_t} = 0.$$

So distance error at each timestep e_t can be normalized by multiplying with weight

$$w_t = \left(\frac{1}{B} \sum_{b=1}^B \mathcal{L}_{\text{reg}b;t} \right)^{-1},$$

where b is the index of data item in mini-batch and B is the batch size.

C. Expert Log Decomposition

In order to obtain decision components in the trajectory logs and selectively study them, we can decompose them through mathematical analysis tools. Fourier transform is a commonly used analysis method. It extracts the coefficient of the signal at different frequencies by convolution signal with sine and cosine functions as basis functions. However, since sine and cosine functions are infinitely supportive, this decomposition will completely lose the time domain characteristics of the signal, resulting in our failure to select part of a certain time segment in each domain component. To achieve time dependent decomposition of trajectories, we propose the following two approaches.

1) *Downsampling within Horizon (DWH)*: In this method, we do not utilize any signal feature extracting operation. But only downsample and truncate the limited horizon of future time steps of expert trajectory iteratively. The downsampling and truncation operations are adopted N times to be aligned with details generated by the NN. Mathematically,

$$\mathcal{T}_{l*} = \mathcal{T} \downarrow 2^{l-1},$$

$$\mathcal{T}_l = \mathcal{T}_{l*:H},$$

where H is the Horizon of decision in each detailing level l .

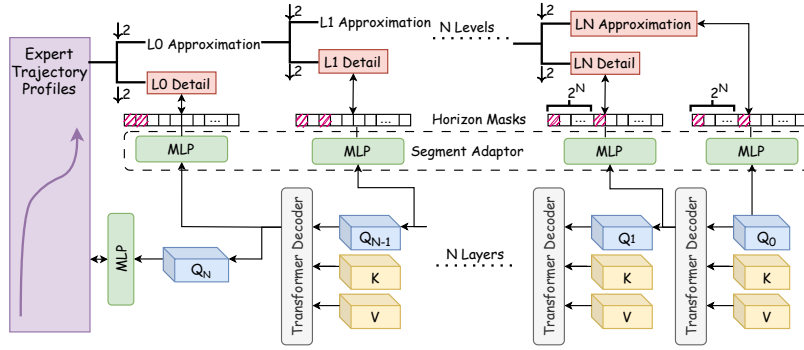


Fig. 4. The iterative detail decoder's architecture leverages reference lane encoding as the initial query for multi-layer attention mechanisms. Detail coefficients extracted during each iteration are integrated with the preceding query to formulate the subsequent query, thereby refining the extraction of further detailed information. The initial query serves as an approximation, with the first query and the ensuing generated details being processed by an MLP. These detail embeddings are then mapped and compared against the detailed components at each level of details. Notably, the horizon masks can be configured individually across levels.

2) *Wavelet Decomposition*: Wavelets, also known as scale-varying basis functions, refer to a method of decomposing signals using compact supporting functions as basis functions. For example, the Haar wavelet, the simplest basis function of the wavelet transformation, enjoys widespread application in signal processing. The basic functions of the Haar wavelet are

$$\phi(t) = \begin{cases} 1, & 0 \leq t < 1 \\ 0, & \text{otherwise} \end{cases}, \psi(t) = \begin{cases} 1, & 0 \leq t < \frac{1}{2} \\ -1, & \frac{1}{2} \leq t < 1 \\ 0, & \text{otherwise} \end{cases},$$

where t is the discrete time index. We can see that when $t \notin [0, 1]$, the basis function value is 0, which means that the function is compact supporting. Among the basis functions, the scaling function $\phi(t)$, often referred to as the father wavelet, serves as a low-pass filter within the wavelet transform process; the mother wavelet function $\psi(t)$ is primarily utilized for extracting the high-frequency components of a signal. Through the convolution of the original signal with these basis functions, the signal's high-frequency and low-frequency components are isolated. In the trajectory decomposition context, the trajectory approximation coefficient \mathcal{T}_A and the detail coefficient \mathcal{T}_D can be derived by performing the following transformation over the time horizon

$$\mathcal{T}_{At} = \sum_k \mathcal{T}[k] \phi(2t - k), \mathcal{T}_{Dt} = \sum_k \mathcal{T}[k] \psi(2t - k),$$

where $\mathcal{T}[k]$ is the discrete trajectory profile, \mathcal{T}_{At} is the low-frequency approximation coefficient at time index t , \mathcal{T}_{Dt} is the high-frequency detail coefficient at time index t , k can be considered as the convolution handler. For Haar wavelet decomposition, \mathcal{T}_{At} represents the sum of $\mathcal{T}[k]$ and $\mathcal{T}[k+1]$ while \mathcal{T}_{Dt} is the product similarities between $[\mathcal{T}[k], \mathcal{T}[k+1]]$ and $[1, -1]$. This decomposition process is called Discrete Wavelet Transformation (DWT), which can be recursively applied to the approximation coefficient \mathcal{T}_A to achieve multi-level l decomposition. By

$$(\mathcal{T}_A^l, \mathcal{T}_D^l) = \text{DWT}(\mathcal{T}_A^{l-1}),$$

we decompose trajectory profiles into N levels. The profile in our experiments is selected to be coordinate values of waypoints. The approximation obtained in the last level is

nominated as the preliminary decision. With the extraction of a detail component in each level, the length of the data is reduced by half.

D. Detail Generation

Since the decomposed trajectory profile has been obtained, the question arises as to how it can be effectively utilized to guide the supervision of the model training process.

1) *Multi-head Detail Decoder (MDD)*: This method leverages the function-fitting ability of MLP to keep gradients. As shown in Fig. 3 (b), the transformer decoder layer generates trajectory embedding. MLPs are utilized to remap trajectory embedding to details of designated levels and the overall approximation. Mathematically,

$$\tilde{\mathcal{T}}_A^N = \text{MLP}(\mathcal{Q}_N), \tilde{\mathcal{T}}_D^l = \text{MLP}_l(\mathcal{Q}_N).$$

2) *Iterative Detail Decoder (IDD)*: To facilitate the learning of detailed information, IDD is designed, which is capable of progressively generating details across multiple iterations as shown in Fig. 3 (c). The architecture of the IDD is depicted in Fig. 4. In the decoding process, the embedding of the reference lane serves as the query \mathcal{Q}_0 , and scenarios encoding E_{sce} serves as the key and value for a series of self-attention operations. We hypothesize that the multi-layer transformer decoder as a trajectory refining process. This hypothesis is based on the observation that the layer normalization operation within each decoding layer reduces information capacity while enhancing accuracy. The embedding extracted at each iteration are accumulated with the previous query, which is then utilized as the subsequent query. Mathematically, the process can be described as

$$\mathcal{Q}_i = \text{TransformerDecoder}(\mathcal{Q}_{i-1}, E_{sce}, E_{sce}).$$

In the decoding process, the transformed feature \mathcal{Q}_i is generated during each iteration and recorded. Logged $\{\mathcal{Q}_i\}$ is adapted by level-wise MLP decoders, i.e.,

$$\tilde{\mathcal{T}}_A^N = \text{MLP}_A(\mathcal{Q}_0), \tilde{\mathcal{T}}_D^l = \text{MLP}_l(\mathcal{Q}_l).$$

The length of $\tilde{\mathcal{T}}$ is the same as planning steps. To make sure the decoded details in same length as driving details, downsampling is performed on $\tilde{\mathcal{T}}$ by

$$\mathcal{T}_A^N = \tilde{\mathcal{T}}_A^N \downarrow 2^N, \mathcal{T}_D^l = \tilde{\mathcal{T}}_D^l \downarrow 2^{l+1}.$$

TABLE I
PRELIMINARY EXPERIMENTS

Detail Gen.			Supervision			Remarks	CLS-NR
#	Iterrative	Detail heads	Horizon	DWT	DWH		
1	-	-	80	-	-	PLUTO, m6	83.28%
2	-	-	10	-	-	Truncation	80.12%
3	-	-	20	-	-	Truncation	87.92%
4	-	-	40	-	-	Truncation	85.22%
5	-	-	-	-	-	Time decay, $l = e, p = 1$	88.36%
6	-	-	-	-	-	Time norm	87.97%
7	-	-	-	-	-	Time norm+contras	92.22%
8	-	✓	10	-	✓	-	85.52%
9	✓	-	10	-	✓	-	82.43%
10	-	✓	10	✓	-	Position	82.26%
11	✓	-	10	✓	-	Position	84.71%
12	-	✓	20	✓	-	Position	82.48%
13	✓	-	20	✓	-	Position	82.96%

These details are compared with the corresponding components of expert trajectories at multiple levels. To get decision details in a proper scope, only limited time horizon H_l of \mathcal{T}_D^l at level l are within the decision scope, supervising model training by

$$\mathcal{L}_{ds} = \frac{1}{N+1} \left(\sum_{l=0}^N \left(\|\mathcal{T}_D^l[:H_l] - \hat{\mathcal{T}}_D^l[:H_l]\|_2 \right) + \|\mathcal{T}_A^N - \hat{\mathcal{T}}_A^N\|_2 \right).$$

IV. EXPERIMENTS

A. Implementation Details

Our training is carried out in the nuPlan dataset [2], which comprises a training set of 25,000 scenarios. We evaluate our model’s performance against baseline models within the nuPlan challenge framework. In addition, we conduct an ablation study to determine the significance of each component within our model. The training is performed on a server equipped with 8 NVIDIA L20 GPUs. We employ the Adam optimizer, with a start learning rate of 0.001, 3 warm-up epochs, and a batch size of 32 for each GPU node, over the course of 25 training epochs. The PyTorch library is utilized for the model’s implementation, with each training session approximately lasting 2 days.

Our evaluation is conducted on the **Val14** [23] subset of the nuPlan dataset, encompassing 1,090 validating scenarios. Each simulation entails a 15-second rollout at a frequency of 10 Hz. The evaluation score is derived using the official evaluation script provided by the nuPlan challenge. Our primary comparison metric is the CLS-NR driving score, which is more challenging as other vehicles do not avoid collisions with the ego vehicle. Besides, the future steps of our model is 80 while the history steps is 21. Both our model and **PLUTO** [19] are set to generate 6 modal trajectories. In our experiments, the maximum horizons of decision scope across levels are controlled by setting **DS Horizon**, which is denoted as h . Furthermore, we borrow the idea in [24] to facilitate the rapid implementation and execution of wavelet transformation in our experiments.

B. Preliminary Experiments

In order to identify truly effective strategies from the ones we explored, extensive comparative experiments are conducted. In these studies, all models are trained on 20% of the dataset for 35 epochs and evaluated on the **Random14** [23] test set, comprising 249 scenarios. The results are shown in Table I. The ablation study encompasses the following configurations: In the first experiment, we train the baseline model without additional peripheral losses, achieving a CLS-NR score of 83.28%. Rows 1–4 are designed to explore the existence of the PlanScope problem. In these experiments, we apply a Time Truncation Horizon of 10, 20, 40, and 80 time steps, respectively. The corresponding results are 80.12%, 87.92%, 85.22%, and 83.28%. The initially rising and subsequently falling score suggests that a planning horizon of 20 is relatively optimal. This corroborates our hypothesis that short-term decisions can improve planning performance. However, overly myopic decisions may introduce other issues, such as collisions due to the absence of predictive planning. Results from rows 5–7 demonstrate that weighting the regression loss enhances planning performance in closed-loop simulations. Specifically, the Decreasing Certainty weight is denoted as *timedecay*, and Time-Dependent Normalization is denoted as *timenorm*. The demonstrated value of p and l *timedecay* achieves best performance in our preliminary grid search. Row 7 shows *timenorm* is of good compatibility with the contrastive loss. Comparisons in rows 8–11 indicate that the Multi-head Detail Decoder exhibits better compatibility with DWH than IDD, while IDD performs well in learning supervision signals obtained via DWT. Additionally, the comparison of rows 10–13 shows that the combination of IDD and DWT achieves relatively better performance when the DS Horizon is set to 20.

C. Comparison with Baselines

We conduct a comparative analysis of our method against several standard approaches, the comparative results are presented in Table II. **Log-Replay**, which entails a straightforward replay of expert trajectories, serves as a baseline reference. This demonstrates the capability of our simulator to accurately

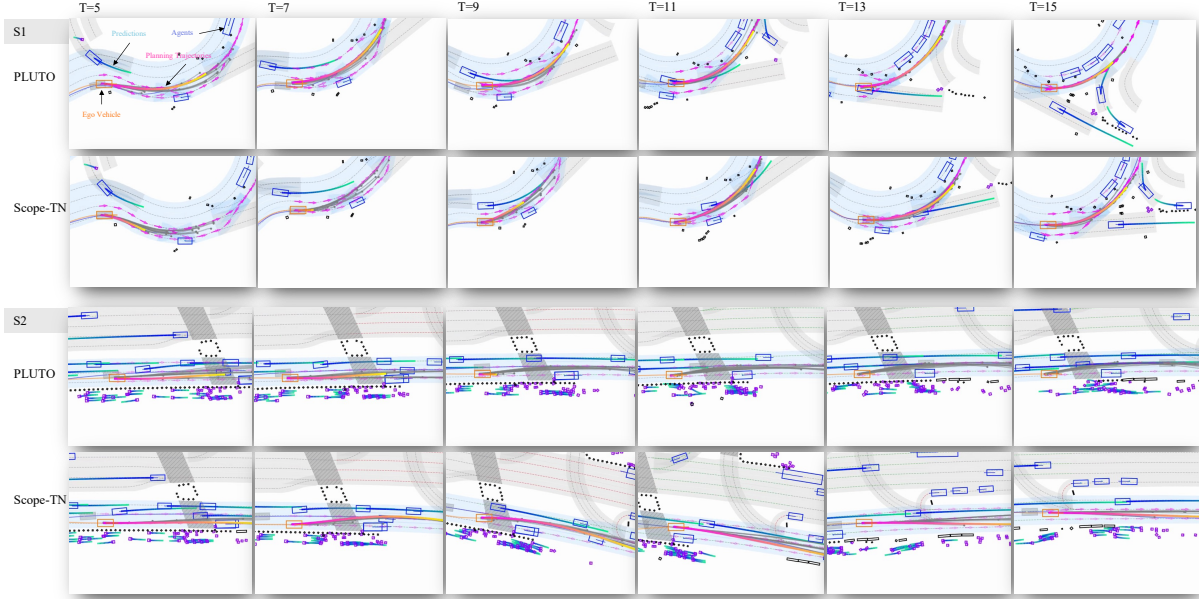


Fig. 5. The qualitative comparison is conducted between the standard PLUTO and PlanScope (Scope) with time dependent normalization (TN), whose quantitative results listed in Table II fourth and third row from bottom respectively. In scenario **S1**, **PLUTO** fails to make a timely response to the impending collision in the short-term, but chooses to continue along the long-term decision, while **Scope** makes a timely yielding maneuver. In scenario **S2**, **PLUTO** adopts a conservative decision due to the high uncertainty of the future trajectory caused by interaction with the rear vehicle in a long time horizon, while **Scope** adopts human-like lane change decision.

TABLE II
COMPARISON WITH BASELINE METHODS

Planner	Comfortness	Progress	w/o Collision	in Speed Limit	Drivable	TTC	CLS-NR	CLS-R
Log-Replay	99.27%	98.99%	98.76%	96.47%	98.07%	94.40%	93.68%	81.24%
IDM	79.31%	86.16%	90.92%	97.33%	94.04%	83.49%	79.31%	79.31%
RasterModel	81.64%	80.60%	86.97%	98.03%	85.04%	81.46%	66.92%	64.66%
UrbanDriver	100.00%	80.83%	94.13%	91.58%	90.83%	80.28%	67.72%	64.87%
GameFormer	93.39%	89.04%	94.32%	98.67	94.87%	86.77%	82.95%	83.88%
PLUTO-m6	95.14%	87.13%	94.45%	97.87%	98.90%	90.92%	85.81%	76.45%
PlanScope-Ih10-DWT	95.96%	86.04%	95.37%	98.20%	98.44%	91.74%	85.99%	75.81%
PlanScope-Mh10-DWH	96.42%	88.72%	95.73%	98.17%	98.72%	92.66%	87.77%	75.39%
PlanScope-Mh20-DWT	97.89%	86.70%	93.72%	98.42%	98.81%	91.28%	85.80%	77.60%
PlanScope-Th20	99.27%	76.32%	95.50%	99.22%	99.36%	91.93%	83.86%	83.74%
PlanScope-timedecay	96.24%	86.34%	95.14%	98.24%	99.63%	91.56%	86.48%	75.22%
PlanScope-timenorm	98.26%	88.04%	96.28%	98.20%	99.45%	92.94%	88.41%	75.56%
PLUTO-m12-C	96.41%	93.28%	96.18%	98.13%	98.53%	93.28%	89.04%	80.01%
PlanScope-timenorm-m12-C	97.25%	89.54%	97.29%	98.04%	99.72%	93.85%	91.32%	80.96%
PLUTO-m12-C-H	91.93%	93.65%	98.30%	98.20%	99.72%	94.04%	93.21%	92.06%
PlanScope-timenorm-m12-C-H	93.85%	93.09%	98.35%	98.22%	99.82%	94.86%	93.59%	91.07%

The suffixes **m6/m12** denote that the trajectory mode number is set to 6 or 12, respectively. **Ih10** abbreviates IDD with a DS Horizon of 10, while **Mh10** refers to MDD with a DS Horizon of 10. **Th20** signifies the use of Time Truncation weights with a DS Horizon of 20. **C** denotes the application of contrastive learning. **H** represents a hybrid method combining learning and rule-based post-processing. **CLS-R** represent Reactive Closed Loop Simulation.

assess the performance of planning algorithms. **IDM** [25] employs the Intelligent Driver Model to maintain safe distances from other agents and adhere to the reference lane. **RasterModel**, introduced in [2], is a CNN-based planning model. **UrbanDriver** [26] is a vectorized planning model leveraging PointNet based polyline encoders and transformer architecture. **PLUTO** [19], our primary baseline, achieves state-of-the-art performance in the nuPlan planning challenge in April 2024. To save computing resources, the multimodal trajectory mode number is set to m6 at first. By default, we have excluded the rule-based trajectory selector, thereby demonstrating that our new model enhances the performance

of the neural planner. Besides, we also eliminate the contrastive learning module, which is empowered by rule-based positive and negative sample construction. These modules are eliminated to reduce artifacts that may introduce bias in results. Our model, designated as **PlanScope**, is evaluated with various modules performs well in preliminary experiments. Part of qualitative comparison is depicted and introduced in Fig. 5. The results in the table indicate that incorporating *timenorm* further enhances PLUTO’s performance in closed-loop simulations, achieving a total score of 93.59%. This improvement is primarily constrained by the capabilities of the post-processing module. Under a framework that relies

solely on network-based output without post-processing, our closed-loop total score 91.32% increases by 2.28% compared to the previous result. In experiments with mode number equals 6 and without contrastive learning, the model with *timenorm* also achieves best CLS-NR score to 88.41%, which increases 2.6% compared to PLUTO-m6. We also observe that the score for *Time Truncation* is lower than the baseline, suggesting that a decision-making strategy focused solely on the short term may overlook critical long-term aspects. Additionally, methods based on detail generation and decomposition show slight improvement. More decomposition methods, decomposing measurements, wavelet forms and related research on horizon adaptation might be required to further enhance its performance. Furthermore, we also found that the CLS-R score improved with *Time Truncation*. The specific mechanism that lead to improvements on CLS-R score needs to be further explored.

V. CONCLUSIONS

This paper identifies the decision sequence learning problem and formulates it as PlanScope, which has been overlooked in previous closed-loop simulations. Several approaches for enabling model to extract necessary decisions from log replays are proposed and explored. Among these, the implementation of *timenorm* achieves a state-of-the-art 91.32% CLS-NR score in no-post-processing mode. In the hybrid mode, it reaches a 93.59% CLS-NR score, which also surpasses the baseline. In addition, detail generation modes combined with our proposed decomposition methods show limited improvement. Their performance does not surpass that of *timenorm* and *timedecay*. Nonetheless, wavelet transformation emerges as a potential solution to this issue. We present these findings as a starting point to narrow down the exploration range for future research. In future work, we plan to conduct more thorough experiments to explore the mechanisms underlying this problem, including further investigation of combinations and loss balancing across levels of detail.

REFERENCES

- [1] S. Grigorescu, B. Trasnea, T. Cocias, and G. Macesanu, "A survey of deep learning techniques for autonomous driving," *Journal of Field Robotics*, vol. 37, no. 3, pp. 362–386, 2020.
- [2] H. Caesar, J. Kabzan, K. S. Tan, W. K. Fong, E. Wolff, A. Lang, L. Fletcher, O. Beijbom, and S. Omari, "nuPlan: a closed-loop ML-based planning benchmark for autonomous vehicles," in *Proceedings of the IEEE/CVF Conference on Computer Vision and Pattern Recognition ADP3 Workshop*, 2021.
- [3] M. Hoerger and H. Kurniawati, "An on-line POMDP solver for continuous observation spaces," in *Proceedings of the IEEE International Conference on Robotics and Automation*, 2021, pp. 7643–7649.
- [4] Y. Lee, P. Cai, and D. Hsu, "MAGIC: Learning Macro-Actions for Online POMDP Planning," in *Proceedings of the Robotics: Science and Systems*, 2021.
- [5] W. Ding, L. Zhang, J. Chen, and S. Shen, "Epsilon: An efficient planning system for automated vehicles in highly interactive environments," *IEEE Transactions on Robotics*, vol. 38, no. 2, pp. 1118–1138, 2021.
- [6] Y. Chen, J. Cheng, S. Wang, H. Liu, X. Mei, X. Yan, M. Tang, G. Sun, Y. Wen, J. Cai, et al., "Enhancing campus mobility: Achievements and challenges of the snow lion autonomous shuttle," *IEEE Robotics & Automation Magazine*, 2024.

- [7] Y. Pan, Q. Lin, H. Shah, and J. M. Dolan, "Safe planning for self-driving via adaptive constrained ILQR," in *Proceedings of the IEEE/RSJ International Conference on Intelligent Robots and Systems*, 2020, pp. 2377–2383.
- [8] J. Mercat, T. Gilles, N. El Zoghby, G. Sandou, D. Beauvois, and G. P. Gil, "Multi-head attention for multi-modal joint vehicle motion forecasting," in *Proceedings of the IEEE International Conference on Robotics and Automation*, 2020, pp. 9638–9644.
- [9] A. Graps, "An introduction to wavelets," *IEEE Computational Science and Engineering*, vol. 2, no. 2, pp. 50–61, 1995.
- [10] M. Medhat, A. Albdel-hafiez, M. Hassan, M. Ali, and Z. Awaad, "A review on applications of the wavelet transform techniques in spectral analysis," in *Proceedings of the Conference on Nuclear and Particle Physics*, 2004.
- [11] A. H. Masquelin, N. Cheney, C. M. Kinsey, and J. H. Bates, "Wavelet decomposition facilitates training on small datasets for medical image classification by deep learning," *Histochemistry and Cell Biology*, vol. 155, no. 2, pp. 309–317, 2021.
- [12] Y. Zheng, S. He, R. Yi, F. Ding, B. Ran, P. Wang, and Y. Lin, "Categorizing car-following behaviors: wavelet-based time series clustering approach," *Journal of Transportation Engineering, Part A: Systems*, vol. 146, no. 8, p. 04020072, 2020.
- [13] B. I. Kwak, M. L. Han, and H. K. Kim, "Driver identification based on wavelet transform using driving patterns," *IEEE Transactions on Industrial Informatics*, vol. 17, no. 4, pp. 2400–2410, 2021.
- [14] R. V. Cowlagi and P. Tsiotras, "Multiresolution motion planning for autonomous agents via wavelet-based cell decompositions," *IEEE Transactions on Systems, Man, and Cybernetics, Part B*, vol. 42, no. 5, pp. 1455–1469, 2012.
- [15] Z. Zhou, J. Wang, Y.-H. Li, and Y.-K. Huang, "Query-centric trajectory prediction," in *Proceedings of the IEEE/CVF Conference on Computer Vision and Pattern Recognition*, 2023, pp. 17 863–17 873.
- [16] J. Cheng, Y. Chen, X. Mei, B. Yang, B. Li, and M. Liu, "Rethinking imitation-based planners for autonomous driving," in *Proceedings of the IEEE International Conference on Robotics and Automation*, 2024, pp. 14 123–14 130.
- [17] C. R. Qi, H. Su, K. Mo, and L. J. Guibas, "PointNet: deep learning on point sets for 3d classification and segmentation," in *Proceedings of the IEEE Conference on Computer Vision and Pattern Recognition*, 2017, pp. 652–660.
- [18] J. Cheng, X. Mei, and M. Liu, "Forecast-MAE: self-supervised pre-training for motion forecasting with masked autoencoders," in *Proceedings of the IEEE/CVF International Conference on Computer Vision*, 2023, pp. 8679–8689.
- [19] J. Cheng, Y. Chen, and Q. Chen, "PLUTO: push the limit of imitation learning-based planning for autonomous driving," *arXiv preprint arXiv:2404.14327*, 2024.
- [20] N. Carion, F. Massa, G. Synnaeve, N. Usunier, A. Kirillov, and S. Zagoruyko, "End-to-end object detection with transformers," in *Proceedings of the European Conference on Computer Vision*, 2020, pp. 213–229.
- [21] R. Xin, J. Cheng, S. Wang, and M. Liu, "Velocity Field: an informative traveling cost representation for trajectory planning," in *Proceedings of the IEEE International Conference on Robotics and Biomimetics*, 2023, pp. 1–6.
- [22] J. Cheng, R. Xin, S. Wang, and M. Liu, "MPNP: Multi-Policy Neural Planner for Urban Driving," in *Proceedings of the IEEE/RSJ International Conference on Intelligent Robots and Systems*, 2022, pp. 10 549–10 554.
- [23] D. Dauner, M. Hallgarten, A. Geiger, and K. Chitta, "Parting with misconceptions about learning-based vehicle motion planning," in *Proceedings of the Conference on Robot Learning*, 2023.
- [24] M. Wolter, F. Blanke, J. Garcke, and C. T. Hoyt, "ptwt - The PyTorch Wavelet Toolbox," *Journal of Machine Learning Research*, vol. 25, no. 80, pp. 1–7, 2024.
- [25] S. Albeaik, A. Bayen, M. T. Chiri, X. Gong, A. Hayat, N. Kardous, A. Keimer, S. T. McQuade, B. Piccoli, and Y. You, "Limitations and improvements of the intelligent driver model," *SIAM Journal on Applied Dynamical Systems*, vol. 21, no. 3, pp. 1862–1892, 2022.
- [26] O. Scheel, L. Bergamini, M. Wolczyk, B. Osinski, and P. Ondruska, "Urban Driver: learning to drive from real-world demonstrations using policy gradients," in *Proceedings of the PMLR Conference on Robot Learning*, 2022, pp. 718–728.